Comparative study of photocatalytic performance of titanium oxide spheres assemblied by nanosized structures

Meinan Liu,[a,*] Jin Chang,[b] Cheng Yan,[a] John M. Bell[a]

[a]*School of Engineering System, Queensland University of Technology, 2 George Street, Brisbane, Queensland 4001, Australia;*

[b]*Chemistry Discipline, Queensland University of Technology, 2 George Street, Brisbane, Queensland 4001, Australia*

Corresponding author. Email: meinan.liu@qut.edu.au

Comparative study of photocatalytic performance of titanium oxide spheres assemblied by nanosized structures

TiO_2 spheres constructed by nanorods, nanoplates and nanosheets have been fabricated by facile hydrothermal/solvothermal methods. Three samples were thoroughly characterized by scanning electron microscopy, X-ray diffraction, Brunauer-Emmett-Teller method and UV spectra. The surface area of spheres assembled by nanosheets is 83.9 m^2g^{-1}, which is larger than that by nanorods (10.8 m^2g^{-1}) and nanoplates (6.31 m^2g^{-1}). The photocatalysis performance, in terms of the decomposition rate of methyl orange, was evaluated in these three samples under UV irradiation. The best photoactivitie was observed in the samples assembled by nanosheets.

Keywords: titanium oxide; hierarchical spheres; photocatalyst

1. Introduction

As an important n-type semiconductor, titanium oxide (TiO_2) has gained increasing attention because of its broad applications in photocatalysis, sensors, dye-sensitized solar cells and self-cleaning coatings [1-5]. Photocatalysis on the surface of TiO_2 is among the most promising technologies for converting solar energy into chemical energy [6-9]. There are four processes in a typical photocatalytic reaction, i.e., generation of electrons and holes by photoexcitation, migration of the photogenerated charge carriers to the surface, subsequent reduction/oxidization of the adsorbed reactants directly by electrons/holes and recombination of the photogenerated electron-hole pairs [6]. It has been widely accepted that a structure with a high specific surface area can promote the photocatalytic processes due to increased reactive sites, such as P25 nanocrystallines [6]. However, in nanocrystallines, the benefit from the size reduction can be compromised by the higher electron-hole recombination rate if the photogenerated electrons and holes can not efficiently move to the surface [6, 7]. To

suppress this recombination process, several strategies have been proposed. Wu et al fabricated anatase TiO_2 nanobelts and they found that one-dimensional structure exhibits a lower electron-hole recombination rate than the nanospheres [6]; Yang et al introduced a stable phase interface by designing a core-shell structure - monoclinic TiO_2 nanofibers coating with a thin shell of anatase TiO_2 nanocrystals, thus enhancing the photocatalytic activity in the nanofibers [7].

Recently, surface scientists found that surface energy has an important impact on the physical properties of materials [10]. In crystalline materials, surface energy is also dependent on crystallographic planes. For example, the average surface energy of anatase TiO_2 is 0.90 J/m^2 for {001}, 0.53 J/m^2 for {100} and 0.44 J/m^2 for {101} [10-13]. Several studies have demonstrated that the highly reactive (001) facets of anatase TiO_2 nanosheets exhibit excellent photocatalytic activity [12, 13]. On the other hand, One problem for those nano unit applications is the difficult separation from the water after the photocatalytic reaction. The construction of hierarchical structure with micro size could solve this nano size problem [14]. These hierarchical structures not only can keep the superior merits from nano unit but also can produce new collective properties and advanced tunable functions arising from nano unit ensembles [15]. Therefore, much attention has been paid to the self-assembly and transformation of nano unit into highly ordered superstructures with controllable architectures and several methods have been developed, such as oriented attachment and spontaneous assembling [16-18].

In this work, we prepared micro spherical TiO_2 architectures constructed by three different nanosized sub units (nanorod, nanoplate and nanosheet) through simple hydrothermal/solvothermal methods. The photocatalysis reaction in these three architectures was investigated.

2. Experiment

2.1 Materials synthesis

2.1.1 TiO_2 spheres assembled by nanorods (sample I)

15 mM titanium isopropoxide (Sigma-Aldrich), 10 mL hydrochloric acid (32 wt%) and 20 mL deionized water were mixed in a Teflon-lined stainless steel autoclave (45 mL volume, Parr Instrument Co.). The synthesis was conducted at 180 °C for 14 h in an electric oven, and then the autoclave was cooled to room temperature naturally. The as-collected powders were washed by deionized water and ethanol for several times, and dried at 80 °C for 5 h.

2.1.2 TiO_2 spheres assembled by nanoplates (sample II)

The synthesis procedure has been reported in our previous work [3]. Briefly, one piece of Ti foil and 15 mL mixed solution of deionized water and dilute hydrofluoric acid (0.2% by weight) were placed into a Teflon-lined stainless steel autoclave. The hydrothermal synthesis was conducted at 130 °C for 10 h in an electric oven.

2.1.3 TiO_2 spheres assembled by nanosheets (sample III)

Nanosheets structure was prepared by a solvothermal method [11]. 1.15 mL titanium isopropoxide (Sigma-Aldrich), 32 mL isopropanol and 0.02 mL diethylenetriamine (DETA) were mixed in a Teflon-lined stainless steel autoclave. The synthesis was conducted at 200 °C for 24 h in an electric oven, and then the autoclave was cooled to room temperature naturally. The as-collected powder was finally treated in the same way as the spheres assembled by nanosheets (2.1.1). To increase the crystallinity, some samples were heated at 400 °C for 3 h in air.

2.2 Materials characterization

The crystal structure of the as-prepared powders was evaluated using X-ray diffraction (XRD, PANanalytical Xpert Pro diffractometer) with Cu Kα radiation (λ = 1.5418 angstrom) in the 2θ range of 10–70°. The morphology of the as-prepared powders was examined by scanning electron microscopy (SEM, FEI Quanta 200). The samples were sputter-coated with gold for 2 min before the observation. An accelerating voltage of 25 kV was used. Transmission electron microscope (TEM, Philips CM200) was also used to examine the detailed morphology. The nitrogen sorption isotherms were measured by volumetric method using an automatic adsorption instrument (Micromeritics, Tristar 3000) at liquid nitrogen temperature (77 K). Specific surface area was calculated by the Brunauer-Emmett-Teller (BET) method from the data in a P/P_0 range between 0.01 and 0.25. UV-Vis adsorption spectra were recorded on UV-Vis-NIR spectrophotometer (Varian Cary 5000).

2.3: Photocatalysis Experiments

The photocatalysis experiments were carried out in a photoreactor equipped with six tubular Hg lamps (NEC, FL20SBL) of 20 W, and the peak of the wavelength was at about 350 nm. A total of 10 mg of TiO_2 catalysts was added to a 10 mL solution of 20 mg/L methyl orange (MO) in a 10 mL polyethylene tube. During irradiation, the tubes were placed onto the carousel inside the photoreactor to ensure the even exposure of each tube to the UV light. At different time intervals of irradiation, the tubes were unloaded and then centrifuged at 10,000 rpm for 3 min to separate the supernate and the catalysts. The supernates were collected and analyzed by recording the characteristic absorption peak of MO (464 nm) using a UV-vis spectrometer (Varian Cary 100).

Based on the UV absorbance as a function of the remaining MO concentration, the efficiency of the MO decomposition was calculated.

3. Results and discussion

The morphologies of the samples are shown in Figure 1. The sample I consists of spheres with an average size of about 3 μm, Fig. 1a. At a high magnification (Figure 1b), it can be seen that the spheres are assembled by nanorods that aggregate together, with a diameter of about 100 nm. It has been proposed that chlorine system can help produce nanorods [2, 3, 19]. In this work, the nanorods with smaller dimensions are firstly formed during the hydrothermal reaction. To reduce the surface energy, these nanorods tend to agglomerate together to form spheres in micro size.

The nanoplates in sample II are shown in Figures 1c and d. These nanoplates are well-defined quadrilateral platelets with smooth surface. These nanoplates are 1-2 μm in size and around 50 nm in thickness. These nanoplates are well assembled into micro spheres with a diameter of about 4 μm. It was suggested that the presence of fluorine can promote the formation of reactive {001} facets [10, 12]. On the basis of the shape-dependent thermodynamic model, the stable exposed facets are {101}, while F-terminated surfaces could result in (001) surface that is more stable than {101} surfaces [10]. Consequently, the nanoplates with reactive {001} facets assembled into micro spheres during this fluorine assisted hydrothermal reaction.

Figures 1e and 1f illustrate the morphology of sample III, which consists of prickly sphere-like structures. The size of these spheres is around 1–3 μm in diameter. It is clear that the spheres are composed of nanosheets, confirmed by a high magnification TEM image (Figure 1d). The thickness of nanosheets is around 10–20 nm. Chen et al reported that tridentate DETA could stabilize the high-energy (001) surfaces and

produce ultrathin nanosheets [11]. In this solvothermal system, with increasing the reaction time, the nanosheets self assembled into hierarchical micro spheres to further reduce the surface energy.

The crystal phases of the as-prepared samples are confirmed by XRD, as shown in Figure 2. Sample I has rutile phase with tetragonal structure, space group $P4_2/mnm$ (JCPDS card, No. 21-1276), while the other two samples contain pure anatase phase with tetragonal structure, space group $I4_1/amd$ (JCPDS card, No. 75-1748). The diffraction peak intensity from sample I and sample II is much higher than that from sample III, which means sample I and II may have a higher crystallinity. To increase the crystallinity in the samples III, as mentioned before, the samples were heated at 400°C for 3 h. This treatment resulted in significant increase of crystallinity in the sample III, Fig. 2. Generally, rutile phase is less catalytic active than anatase phase due to a lower surface affinity with many organic compounds and a higher rate of recombination of photogenerated charge pairs. Recently, it was found that mixed TiO_2 phases exhibit much higher catalytic activity than the individual phases [7, 9]. The well known P25 is a prime example, which consists of 80% anatase and 20% rutile and shows superior photocatalytic activity. Therefore,, these two different phases will be used to study its influence on photocatalysis behaviour.

The surface area of the three samples was measured using the BET method. The N_2 adsorption-desorption isotherms at 77 K and the pore size distribution evaluated by the Barrett-Joyner-Halenda (BJH) method are shown in Figure 3. The isotherm of sample I (Figure 3a) can be classified to be a type III isotherm with a type H3 hysteresis loop at the relative pressure of 0.5–0.9. The BET specific surface area is 10.8 m^2g^{-1}, a total pore volume is around 0.04 cm^3g^{-1} and the average pore diameter by BET is about 14.85 nm. Sample II also shows a type III isotherm with a type H3 hysteresis loop at the

relative pressure of 0.5–0.9. The BET specific surface area is 6.31 m^2g^{-1}, a total pore volume is around 0.03 cm^3g^{-1} and the average pore diameter by BET is about 14.78 nm. Sample III exhibits a type II adsorption isotherm with a type H3 hysteresis loop at the relative pressure of 0.45–0.9, which indicates a mesoporous structure and give rise to a relatively high BET specific surface area of 83.9 m^2g^{-1}, and a total pore volume of 0.126 cm^3g^{-1} and the average pore diameter by BET is about 5.49 nm.

The photocatalytic degradation mechanism of MO by TiO_2 under UV irradiation was illustrated in Figure 4. TiO_2 is a photosensitive material, and when it is irradiated with UV light, electrons in the valence band absorb the photon energy and jump to the conduction band, leaving holes in the valence band [7]. The photogenerated hole can be captured by OH^- or H_2O to produce the hydroxyl radicals. These hydroxyl radicals then oxidize the MO to low molecular weight by products. Generally, the bandgap of anatase TiO_2 is around 3.2 eV and rutile TiO_2 is around 3.0 eV [7]. Optical property of TiO_2 spheres with different sub units has also been studied in this work. As shown in Figure 5, the absorption edge of the sample I, II and III is about 517 nm, 437 nm and 403 nm, respectively, and the corresponding bandgaps are 2.40 eV, 2.84 eV and 3.08 eV. The absorption edge of the sample III after heating at 400 °C is around 393 nm and the corresponding bandgap is about 3.16 eV. Although both sample II and III are anatase phase, the absorption edge of sample III takes an obvious blue shift, around 32 nm, comparing with that of sample II. This may be caused by the quantum effect of those nanosheets shown in Figure 1f. However, the absorption edge of sample III after heated at 400 °C does not take an obvious shift. But in the visible light region, it is clear that there is a significant difference.

The photocatalysis performance of three samples for degradation of MO in an aqueous solution under UV irradiation is shown in Figure 6. Apparently, sample III

exhibits a much higher degradation efficiency compared to the samples I and II. In Figure 6, it can be seen that MO is almost completely degradated by sample III after UV irradiation of 2 h. The high photocatalytic activity of sample III is attributed to the unique structure. As Chen et al reported, a nanosheet structure tends to expose high active (001) facets, with an exposure rate of nearly 100% [11]. In the sample II, the nanoplates also exposes (001) facets, but the rate is around 30% [14], leading to a lower photocatalytic efficiency than the sample III. In addition, the much higher surface area of sample III also provides more active sites for the degradation reaction. The surface area of sample III is about 7.8 and 13.3 times larger than that of the sample I and sample II, respectively. Note that although the surface area of sample I is larger than sample II, its photocatalytic activity is lower than that of sample II. This again confirms that the active (001) facets play a dominating role in improving the photocatalytic performance. Furthermore, the rutile structure in the sample I may be responsible for the low photocatalytic performance due to the high recombination rate [6, 7].

In summary, TiO_2 spheres assembled by nanorods, nanoplates and nanosheets were prepared by simple hydrothermal and solvothermal methods. The photoactivities show that the spheres constructed by nanosheets exhibits the best photocatalytic performance. This may be attributed to the high active (001) facets and higher surface area.

Acknowledgements

M. Liu thanks the financial support from Queensland University of Technology via Vice-Chancellor's Research Fellowship scheme.

References:

[1] O. K. Varghese, M. Paulose, and C. A. Grimes, *Long vertically aligned titania nanotubes on transparent conducting oxide for highly efficient solar cells*, Nature Nanotechnology 4 (2009), pp. 592-597.

[2] M. Liu, H. Wang, C. Yan, G. Will, and J. Bell, *One-step synthesis of titanium oxide with trilayer structure for dye-sensitized solar cells*, Appl. Phys. Lett. 98 (2011), pp.133113.

[3] M. Liu, C. Yan, J. Bell, and G. Will, *Synthesis of superhydrophilic titanium oxide spheres and flowers*, Nanosci. Nanotechnology Lett. 3 (2011), pp. 1-6.

[4] T. Kang, A. P. Smith, B. E. Taylor, and M. F. Durstock, *Fabrication of highly-ordered TiO_2 nanotube arrays and their use in dye-sensitized solar cells*, Nano Lett. 9 (2009), pp. 601-606.

[5] J. Ye, W. Liu, J. Cai, S. Chen, X. Zhao. H. Zhou, and L. Qi, *Nanoporous anatase TiO_2 mesocrystals: additive-free synthesis, remarkable crystalline-phase stability, and improved lithium insertion behaviour*, J. Am. Chem. Soc. 133 (2011), pp. 933-940.

[6] N. Wu, J. Wang, D. N. Tafen, H. Wang, J. Zheng, J. P. Lewis, X. Liu, S. S. Leonard, and A. Manivannan, *Shape-enhanced photocatalytic activity of single-crystalline anatase TiO_2 (101) nanobelts*, J. Am. Chem. Soc. 132 (2010), pp. 6679-6685.

[7] D. Yang, H. Liu, Z. Zheng, Y. Yuan, J. Zhao, E. R. Waclawik, X. Ke, and H. Zhu, *An efficient photocatalyst structure: TiO_2 (B) nanofibers with a shell of anatase nanocrystals*, J. Am. Chem. Soc. 131 (2009), pp. 17885-17893.

[8] X. Lu, S. Ding, Y. Xie, and F. Huang, *Non-aqueous preparation of high-crystallinity hierarchical TiO_2 hollow spheres with excellent photocatalytic efficiency*, Eur. J. Inorg. Chem. 2011 (2011), pp. 2879-2883.

[9] G. Li, N. M. Dimitrijevic, L. Chen, J. M. Nichols, T. Rajh, and K. A. Gray, *The important role of tetrahedral Ti^{4+} sites in the phase transformation and photocatalytic activity of TiO_2 nanocomposites*, J. Am. Chem. Soc. 130 (2008), pp. 5402-5403.

[10] H. G. Yang, C. H. Sun, S. Z. Qiao, J. Zou, G. Liu, S. C. Smith, H. M. Cheng, and G. Q. Lu, *Anatase TiO_2 single crystals with a large percentage of reactive facets*, Nature 453 (2008), pp. 638-642.

[11] J. S. Chen, Y. L. Tan, C. M. Li, Y. L. Cheah, D. Luan, S. Madhavi, F. Y. C. Boey, L. A. Archer, and X. W. Lou, *Constructing hierarchical spheres from large ultrathin anatase TiO_2 nanosheets with nearly 100% exposed (001) facets for fast reversible lithium storage*, J. Am. Chem. Soc. 132 (2010), pp. 6124-6130.

[12] X. Han, Q. Kuang, M. Jin, Z. Xie, and L. Zheng, *Synthesis of titania nanosheets with a high percentage of exposed (001) facets and related photocatalytic properties*, J. Am. Chem. Soc. 131 (2009), pp. 3152-3153.

[13] J. S. Chen, C. Chen, J. Liu, R. Xu, S. Z. Qiao, and X. W. Lou, *Ellipsoidal hollow nanostructures assembled from anatase TiO_2 nanosheets as a magnetically separable photocatalyst*, Chem. Commun. 47 (2011), pp. 2631-2633.

[14] Q. Xiang, J. Yu, and M. Jaroniec, *Tunable photocatalytic selectivity of TiO_2 films consisted of flower-like microspheres with exposed {001} facets*, Chem. Commun. 47 (2011), pp. 4532-4534.

[15] F. Liu and D. Xue, *Assembly of nanoscale building blocks at solution/solid interfaces*, Mater. Res. Bull. 45 (2010), pp. 329-332.

[16] M. Liu and D. Xue, *Large-scale fabrication of $H_2(H_2O)Nb_2O_6$ and Nb_2O_5 hollow microspheres*, Mater. Res. Bull. 45 (2010), pp. 333-338.

[17] J. Liu, H. Xia, D. Xue, and L. Lu, *Double-shelled nanocapsules of V_2O_5-based composites as high-performance anode and cathode materials for Li ion batteries*, J. Am. Chem. Soc. 131 (2009), pp. 12086-12087.

[18] W. Shao, F. Gu, C. Li, and M. Lu, *Interfacial confined formation of mesoporous spherical TiO_2 nanostructures with improved photoelectric conversion efficiency*, Inorg. Chem. 49 (2010), pp. 5453-5459.

[19] B. Liu and E. S. Aydil, *Growth of oriented single-crystalline rutile TiO_2 nanorods on transparent conducting substrates for dye-sensitized solar cells*, J. Am. Chem. Soc. 131 (2009), pp. 3985-3990.

Figure Caption List:

Figure 1. SEM images of spheral architectures of TiO_2 constructed by different sub units. (a, b) nanorods; (c, d) nanoplates; (e) nanosheets. TEM image of TiO_2 spheres assembled by nanosheets (f).

Figure 2. XRD patterns of spheral architectures of TiO_2 with three different sub units: nanorods, nanoplates and nanosheets and TiO_2 spheres constructued by nanosheets heated at 400 °C for 3 h.

Figure 3. N_2 adsorption – desorption isotherms of TiO_2 spheres with three different sub units and the pore size distribution of the corresponding samples.

Figure 4. Schematic diagram showing the energy band structure and electron-hole pair separation in the TiO_2 structure.

Figure 5. UV spectra of TiO_2 spheres constructed by nanoplates, nanorods and nanosheets and TiO_2 spheres constructued by nanosheets heated at 400 °C for 3 h.

Figure 6. Photocatalytic degradation of MO using the as-prepared TiO_2 spheres constructed by nanorods, nanoplates and nanosheets heated at 400 °C for 3 h. C_0 is the initial concentration of MO before UV irradiation.

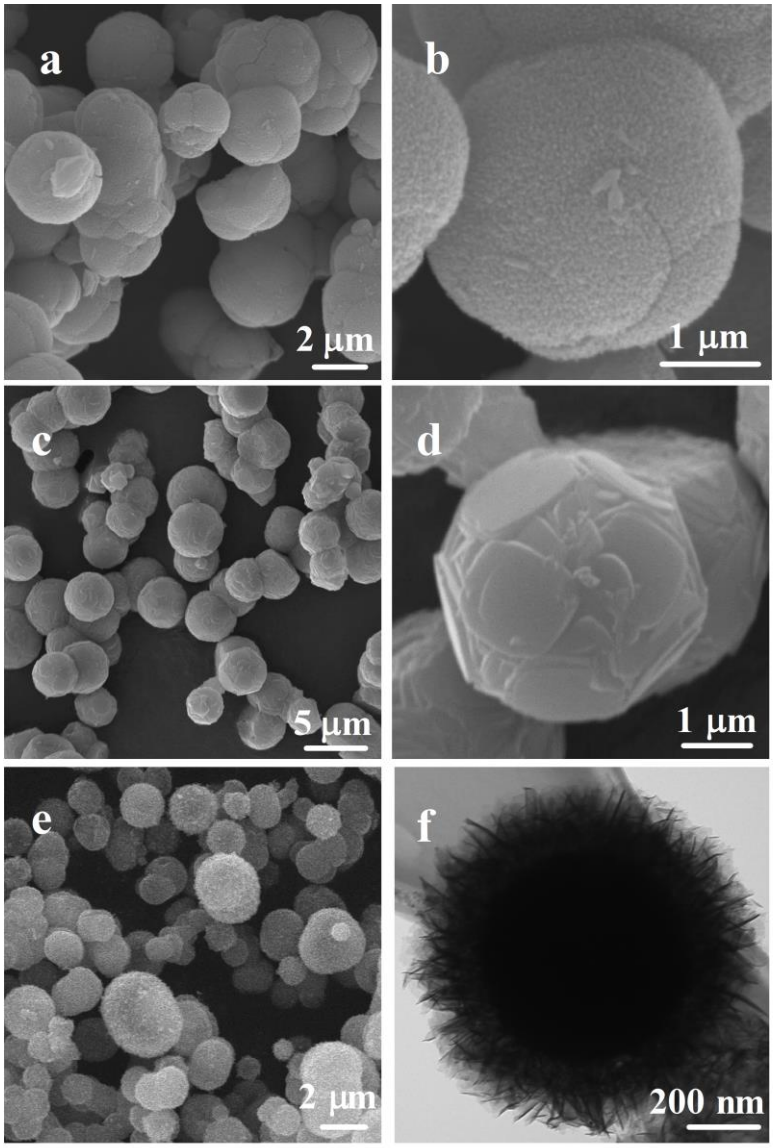

Fig. 1

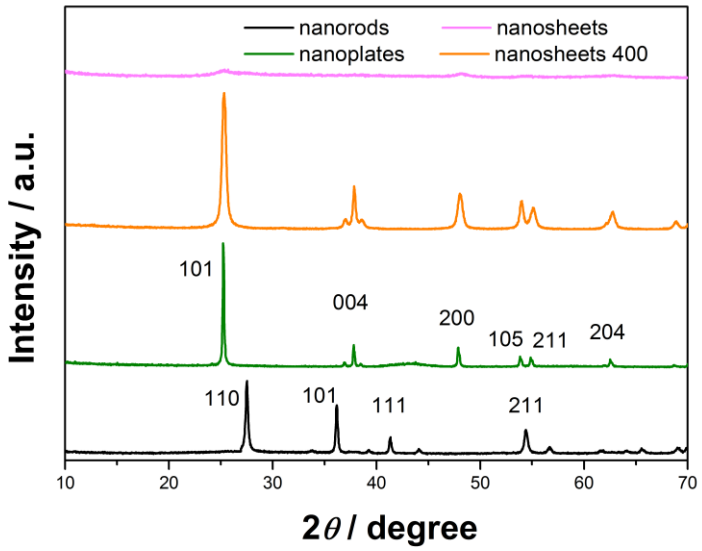
nanorods
nanosheets
nanoplates
nanosheets 400
Intensity / a.u.
101
004
200
105
211
204
110
101
111
211
10
20
30
40
50
60
70
2θ / degree

Fig. 2

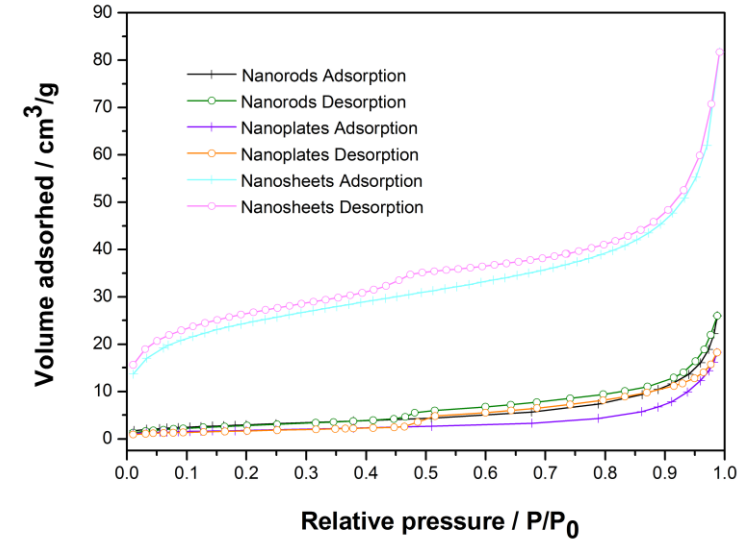
Nanorods Adsorption
Nanorods Desorption
Nanoplates Adsorption
Nanoplates Desorption
Nanosheets Adsorption
Nanosheets Desorption
Volume adsorhed / cm3/g
Relative pressure / P/P0

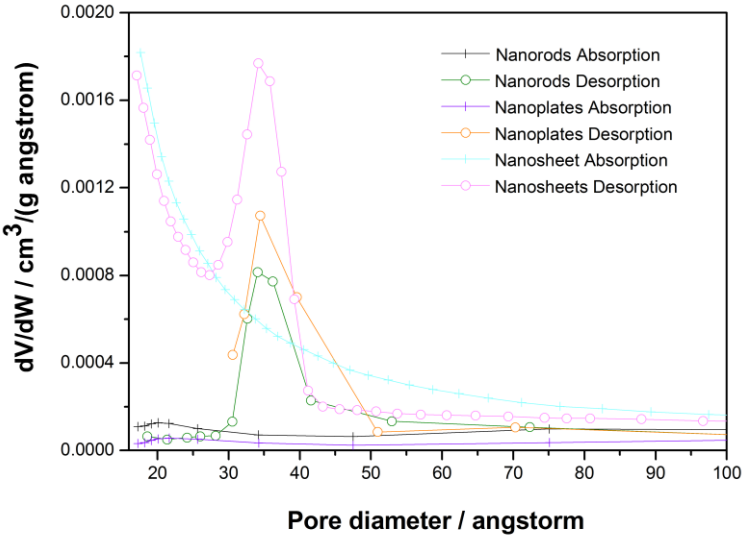
Nanorods Absorption
Nanorods Desorption
Nanoplates Absorption
Nanoplates Desorption
Nanosheet Absorption
Nanosheets Desorption
dV/dW / cm3/(g angstrom)
Pore diameter / angstorm

Fig. 3

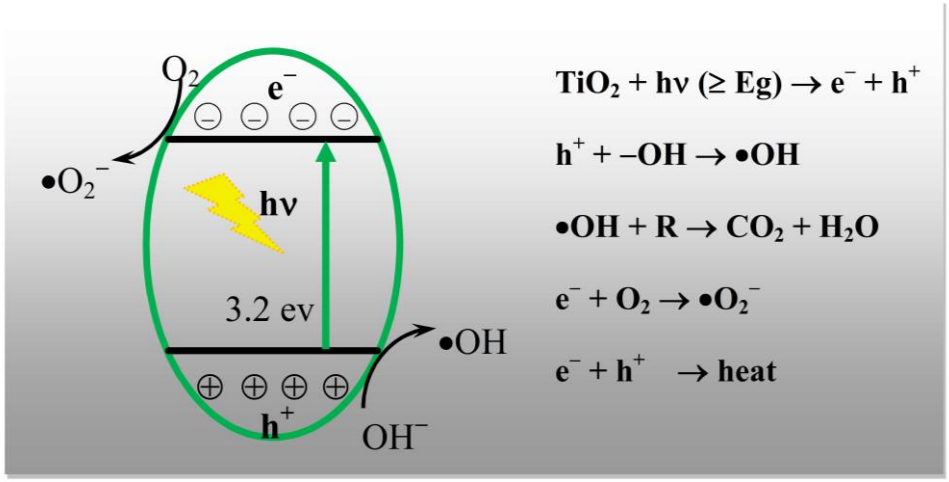
O2
e−
•O2−
hν
3.2 ev
•OH
h+
OH−
TiO2 + hν (≥ Eg) → e− + h+
h+ + –OH → •OH
•OH + R → CO2 + H2O
e− + O2 → •O2−
e− + h+ → heat

Fig. 4

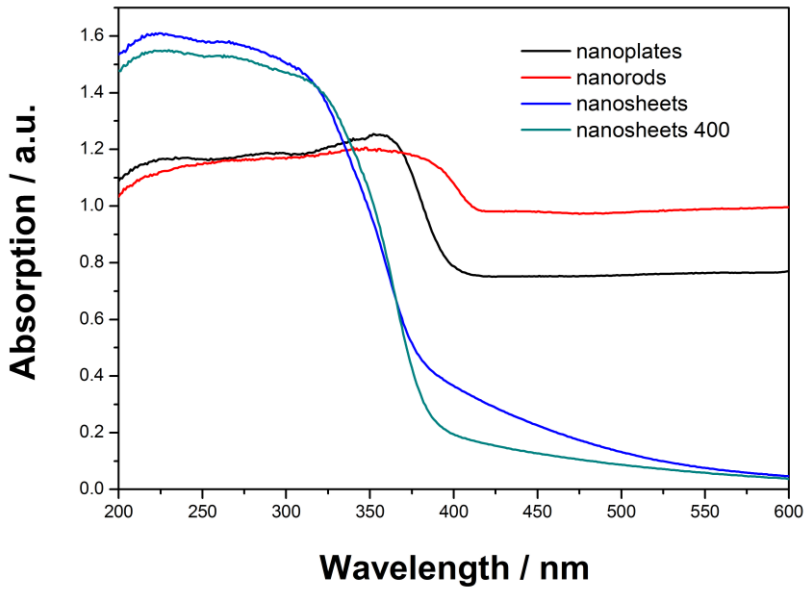
Absorption / a.u.
Wavelength / nm
nanoplates
nanorods
nanosheets
nanosheets 400
0.0
0.2
0.4
0.6
0.8
1.0
1.2
1.4
1.6
200
250
300
350
400
450
500
550
600

Fig. 5

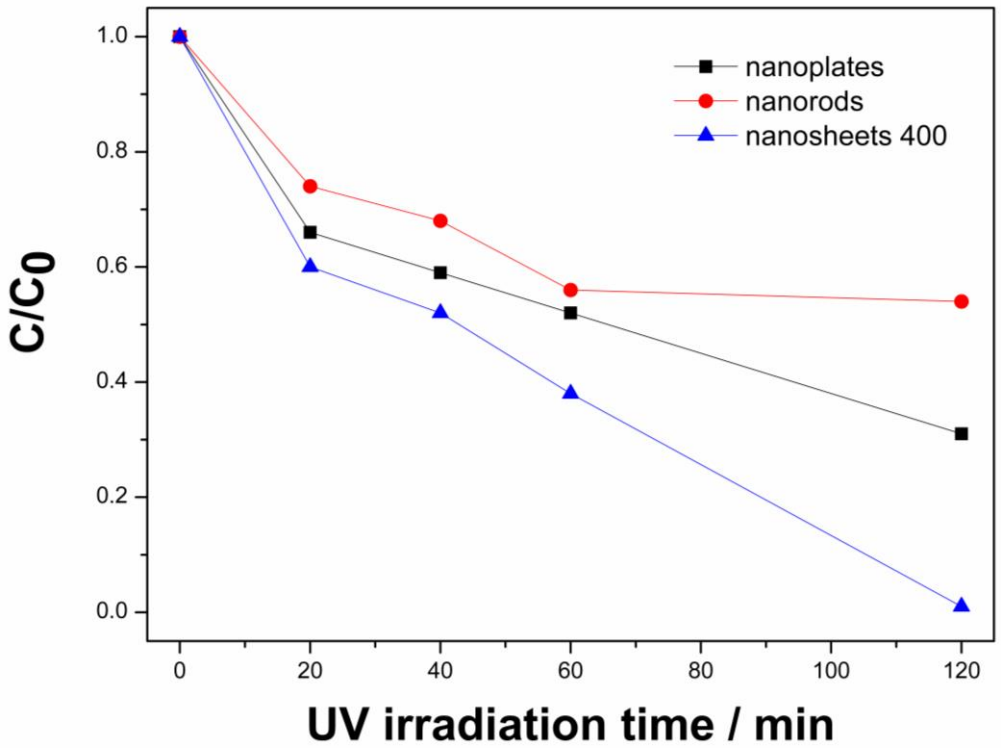
C/C0
1.0
0.8
0.6
0.4
0.2
0.0
0
20
40
60
80
100
120
UV irradiation time / min
nanoplates
nanorods
nanosheets 400